# A Versatile, Highly-efficient Nanofibrous Separation Membrane

*Hua Zhou[a,b], Haitao Niu[a,c], Hongxia Wang[a]*, Weidong Yang[d], Xin Wei[a], Hao Shao[a], Tong Lin[a]**

[a]. Institute for Frontier Materials, Deakin University, Geelong, VIC 3216, Australia
[b]. Institute of Textile and Clothing, Qingdao University, 266000, China
[c]. Collaborative Innovation Center for Eco-Textiles of Shandong Province, Qingdao University, 266000, China
[d]. Future Manufacturing and Flagship, CSIRO, Clayton South, VIC 3169, Australia

Corresponding Authors' emails: tong.lin@deakin.edu.au; hong.wang@deakin.edu.au

# Electronic Supplementary Information

***Materials*:** Nylon-6 pellets, 1,2-Dichloroethane, oil red, oil blue, oil green and formic acid were obtained from Sigma-Aldrich. Capstone FS-60 was provided by DuPont. Spunbond PET nonwoven fabric was purchased from the local supermarket. The PET fabric was cleaned with ethanol and distilled water prior to use. Mineral oil, *n*-hexane, and dimethylformamide were purchased from Chem-Supply Pty Ltd. Diesel was obtained from local Caltex fuel outlet. Nylon-6 solutions were prepared by dissolving nylon-6 pellets in formic acid and stirring for 5 hours at 40 °C. FS-60 solution was prepared by adding 6.0 g FS-60 to 100 ml distilled water and then stirred for 5 min to form a homogenous solution.

***Other characterizations*:** SEM images were taken using an SEM Supra 55VP operated at an acceleration voltage of 5.0 kV. XPS were collected on a VG ESCALAB 220-iXL XPS spectrometer with a monochromated AL Kα source (1486.6 eV) using samples of ~3 $mm^2$ in size. The X-ray beam incidence angle is 0° with respect to the surface normal, which corresponds to a sampling depth of ~10 nm. The XPS spectra were analyzed by the CasaXPS software. Contact angles were measured by a contact angle goniometer equipped with a precision camera to characterize static and dynamic process of water on the fibrous matrix (KSV CAM 101) using liquid droplets of 5 μL in volume. Breakthrough pressure was measured using customer-built equipment comprising a fluid-feeding system with a flow rate controller, a pressure gauge and a sample holder. During measurement, the fluid was loaded on one side of the fibrous membrane at a flow rate of 20 ml/min and the minimum pressure at which the fluid started passing through the membrane was recorded as the breakthrough pressure.

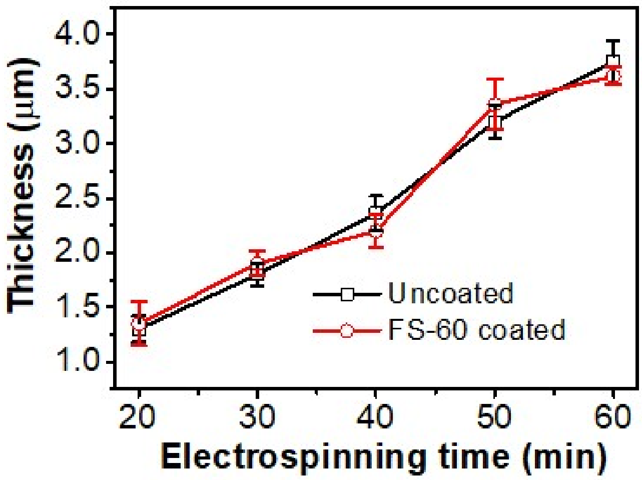


Fig. S1 Nylon-6 nanofibrous membrane thickness changes with electrospinning time before and after the coating treatment.

Nylon-6 nanofibrous membranes of different thicknesses were prepared by adjusting electrospinning time. With increasing electrospinning time form 20 min to 60 min, the membrane thickness increased from 1.30 μm to 3.75 μm. After the coating treatment, the fibrous thickness has no obvious change.

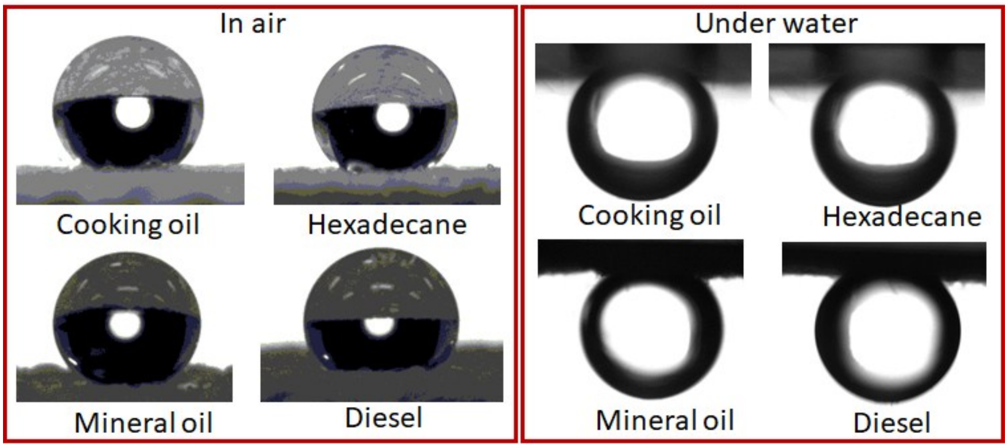

Fig. S2 Photos taken from CA tester showing OCA of the SHI-SOP fibrous membranes in air and underwater states.

Fig. S2 show the oil contact angle (OCA) of the coated fibrous membrane in both air and underwater states. In air (dry state), the membrane showed OCA of 158°, 156°, 152°, and 150° for cooking oil, mineral oil, hexadecane, and diesel, respectively. When the membrane was placed in water, it showed underwater superoleophobicity with underwater oil contact angle (UOCA) of 166°, 168°, 163°, and 162°, respectively.

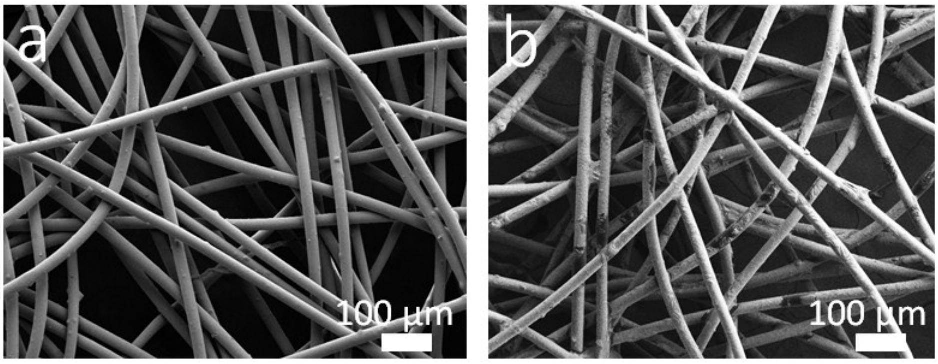

Fig. S3 SEM images of PET spun bound nonwoven substrates: a) before, and b) after FS-60 coating treatment.

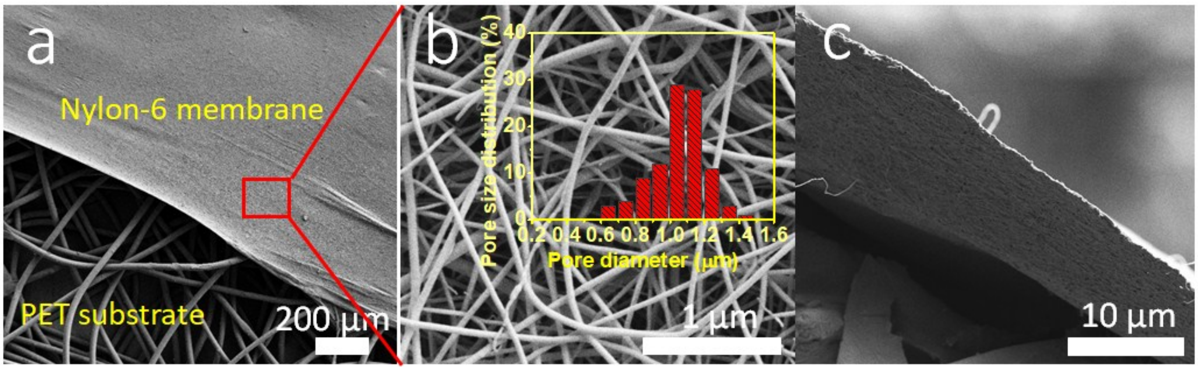

Fig. S4 SEM images of: a, b) top-view of nylon-6/PET composite membrane without coating treatment, c) the cross-section view of nylon-6 nanofibrous membrane without coating treatment. (The inset in b is the diagram of the pore distribution of the nylon-6 layer before coating).

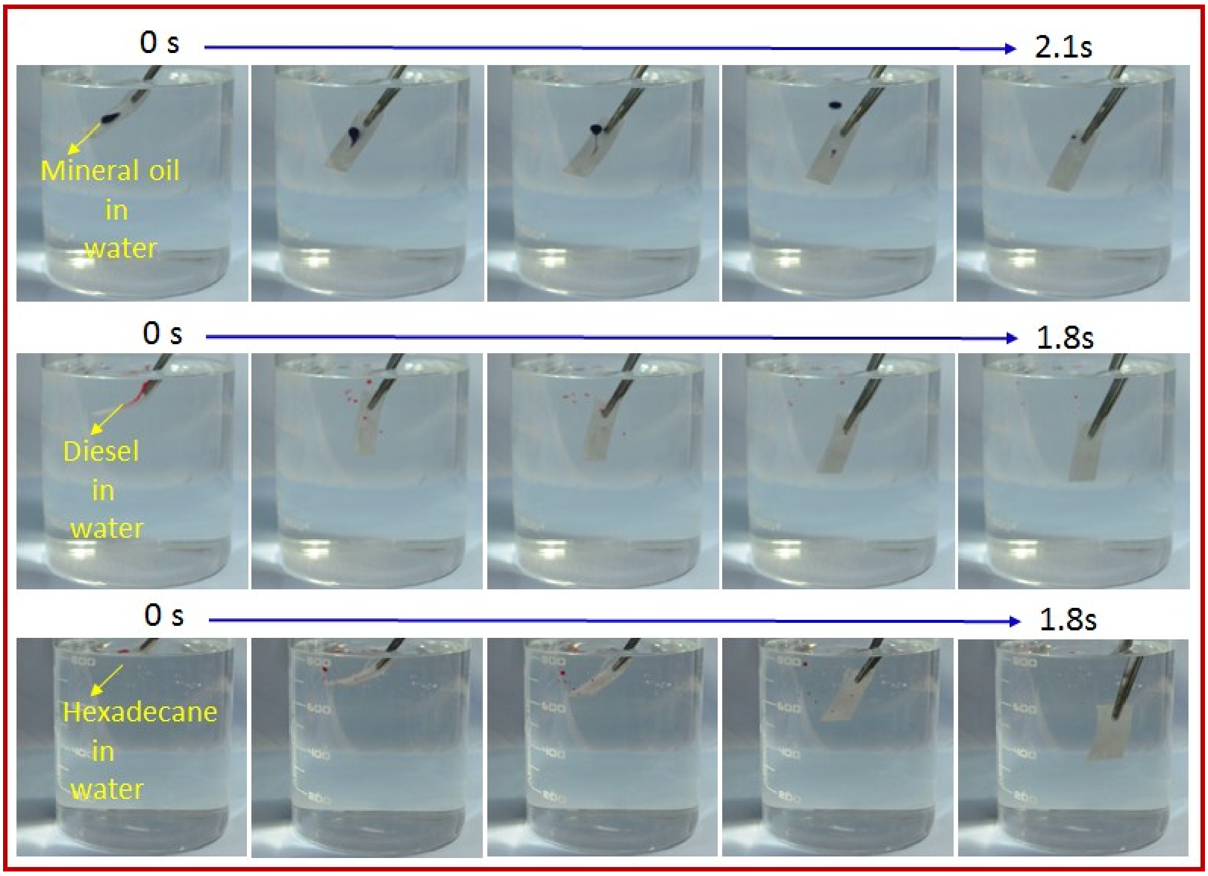

Fig. S5 Snapshots taken from videos to show immersing oil pre-contaminated SHI-SOP membranes in water.

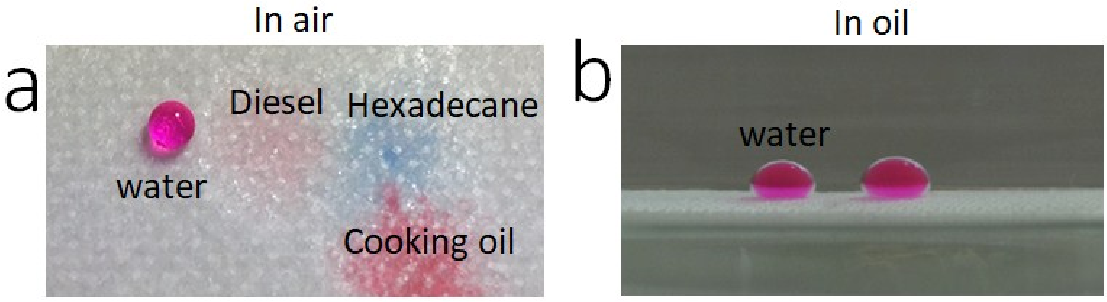


Fig. S6 a) Water and oils droplets on the uncoated nylon-6/PET membrane surface, b) water droplets stayed on the uncoated membrane in oil.

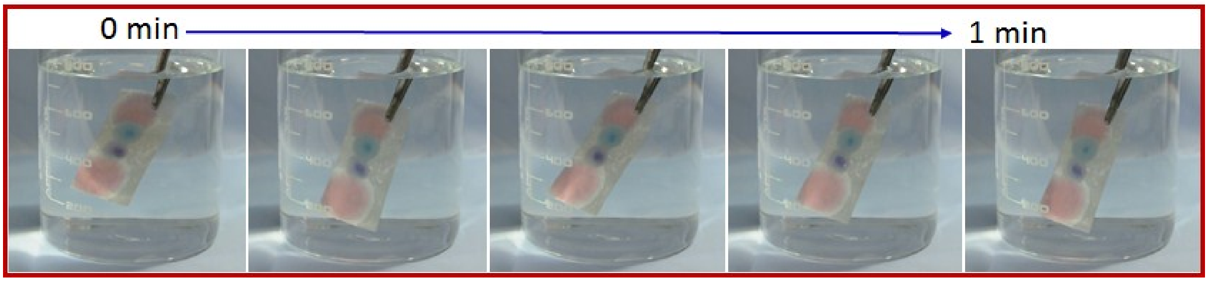

Fig. S7 Snapshots taken from a video to show immersing the oil-contaminated nanofibrous membrane (uncoated) in water (oils from top: red diesel, blue hexadecane, purple mineral oil, and red cooking oil).

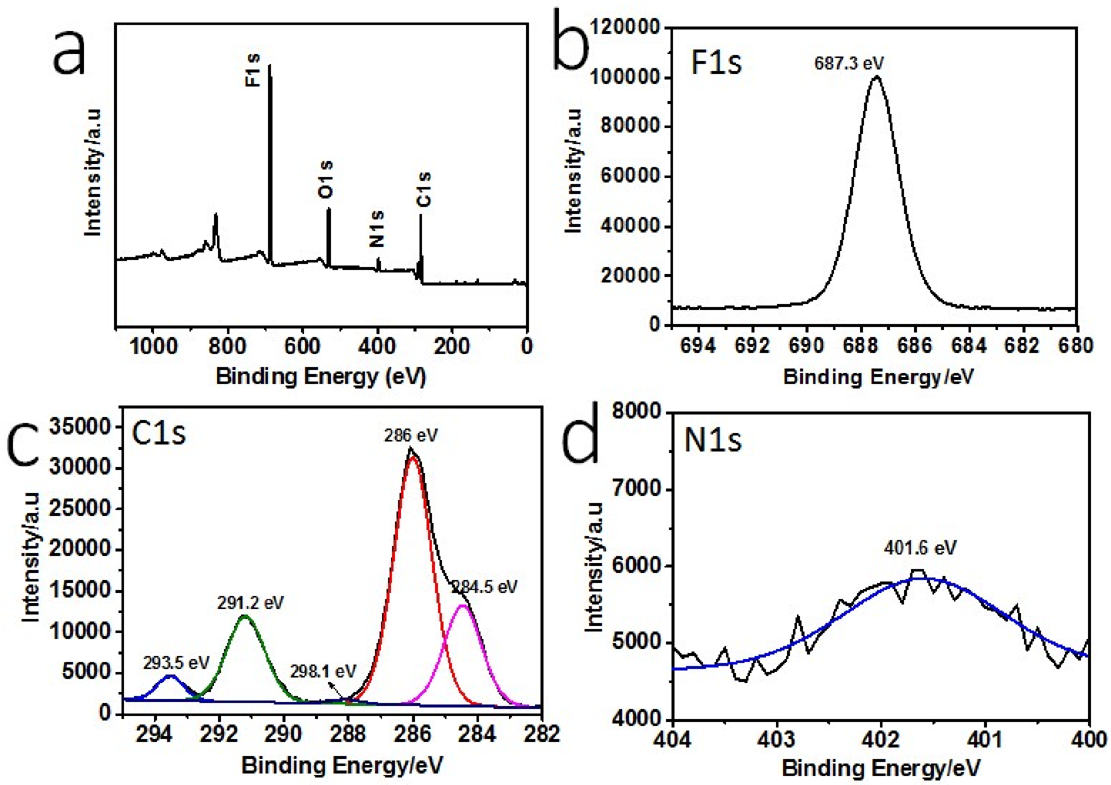


Fig. S8 a) XPS survey of the FS-60 coated nanofibrous membrane, b-d) curved-fitted high resolution c) F1s, d) C1s, and e) N1s spectra of the coated fibrous membrane.

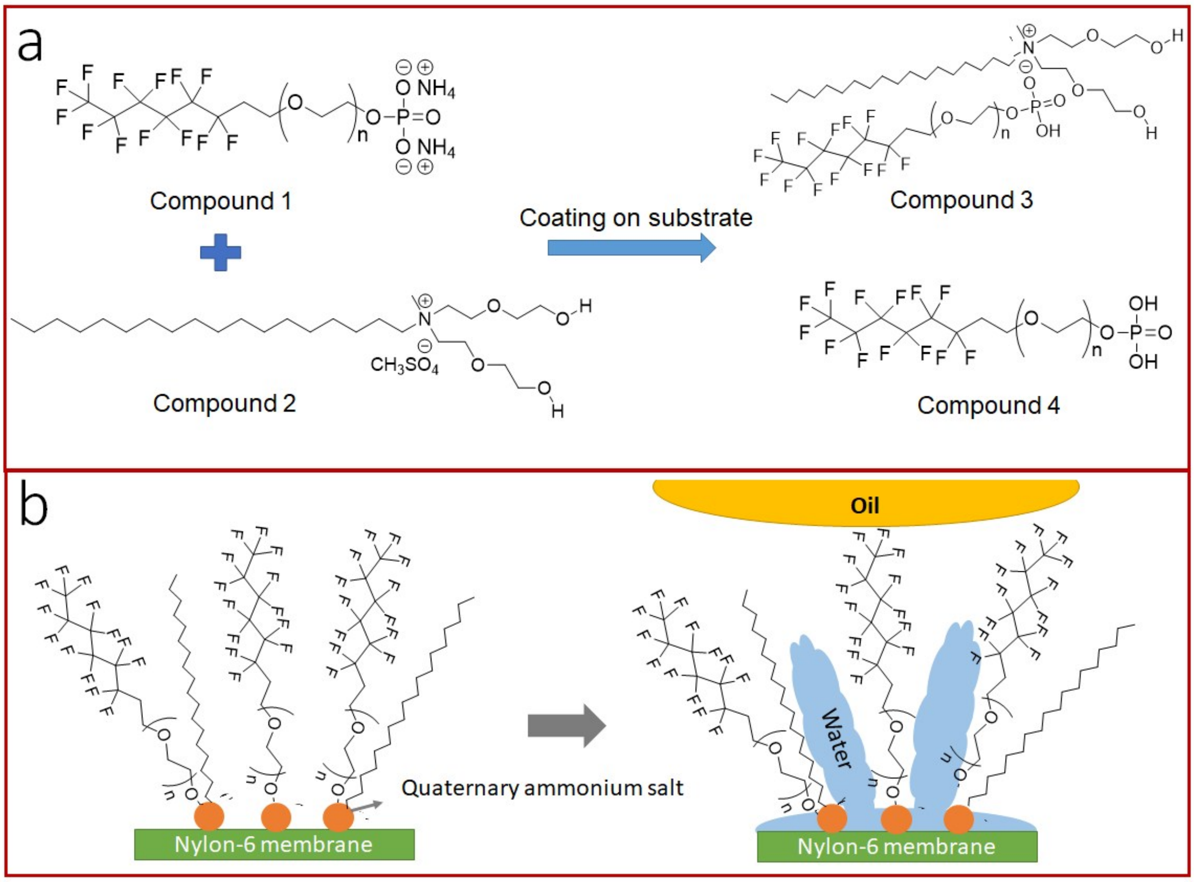


Fig. S9 a) The main chemical compounds in FS-60 and the chemical structures before and after coating on the substrate ($n \geq 4$), b) Schematic illustration of SHI-SOP mechanism on molecular levels.

Fig. S9a show the main chemical compounds in FS-60 and the chemical structures after the coating on the substrate.

The formation of SHI-SOP surfaces was explained by the co-existence of hydrophilic quaternary ammonium groups and low surface energy fluoroalkyl groups on the coating surface. Fig. S9b illustrates the wetting mechanism. In dry state, the fluoroalkyl groups tend to be on top surface because of the ability to reduce the surface free energy. This enables the surface to have low affinity to oil fluid. However, when water is brought to the surface, the strong affinity of the quaternary ammonium groups leads to the surface to be hydrated rapidly, showing hydrophilicity. The inherent surface roughness of the Nylon-6 nanofibrous membrane increases both oleophobicity and hydrophilicity. In underwater, the hydration of the surface makes the surface easy to be wetted with water and this further increases the underwater oleophobicity. However, the existence of a large number of the lipophilic groups restricts swelling of the coating layer.

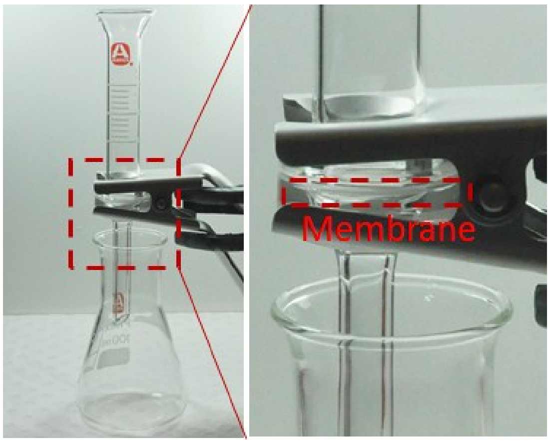

Fig. S10 Experimental set-ups for separation of oil-in-water emulsions.

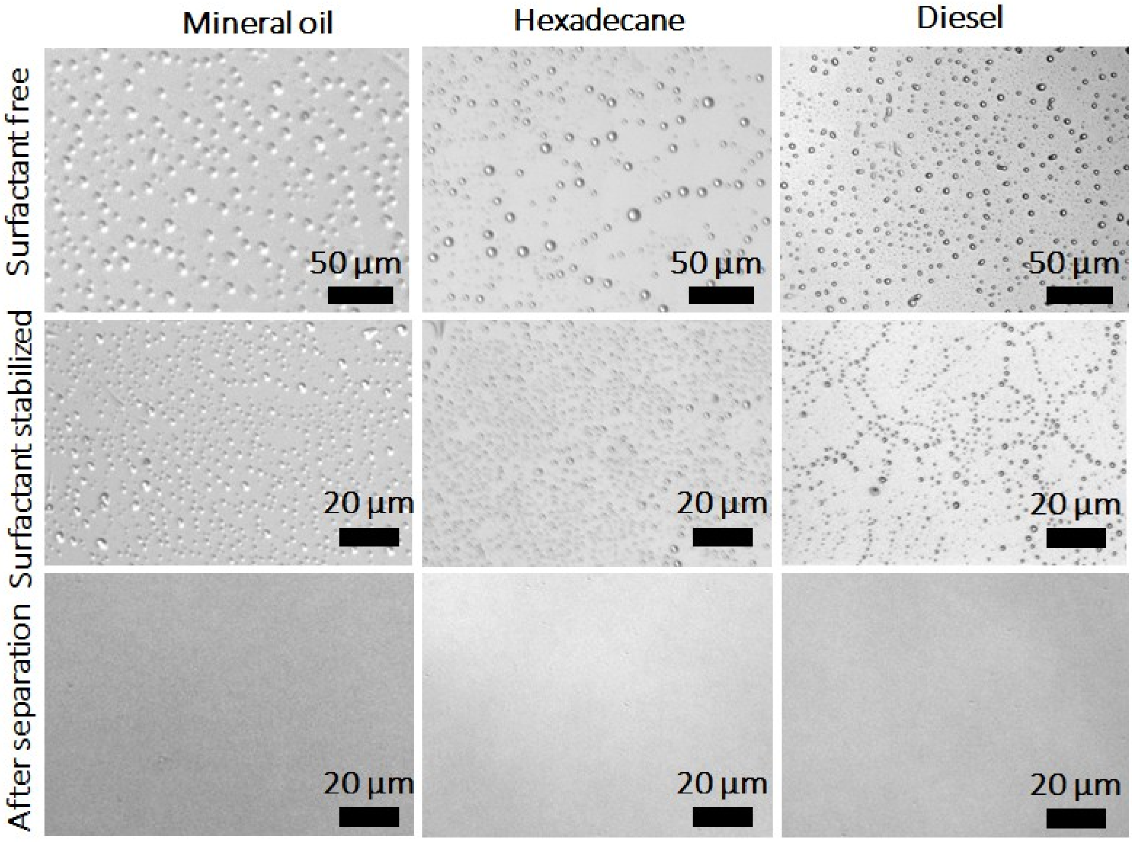

Fig. S11 Optical microscopy images and photos of the SF- and SS-emulsions derived from different oils before and after separation.

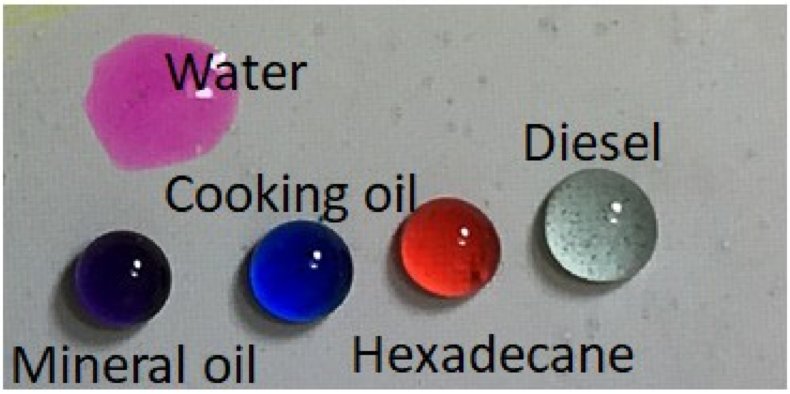


Fig. S12 Water and oil droplets on the FS-60 coated membrane after 10 cycles of oil-water emulsion separation.

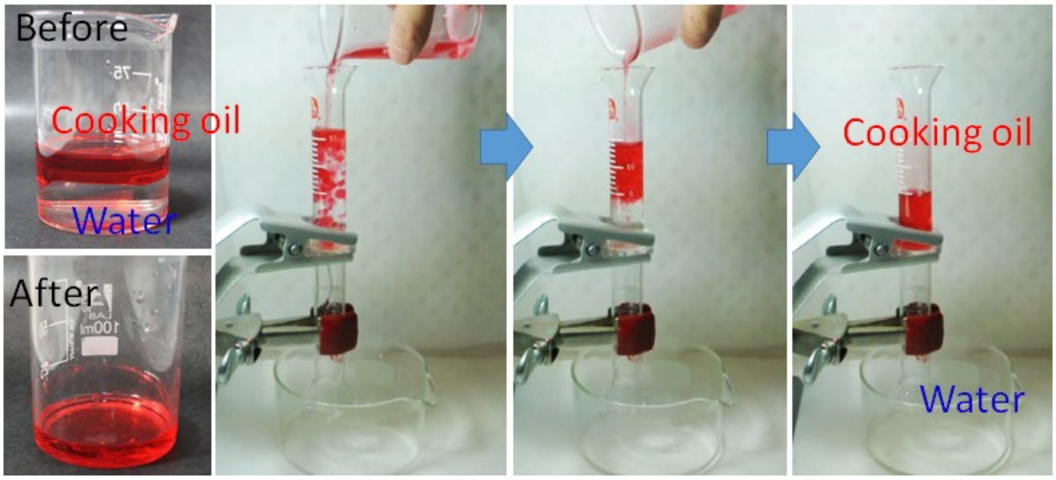

Fig. S13 Photos showing membrane separation of bulk oil from water.

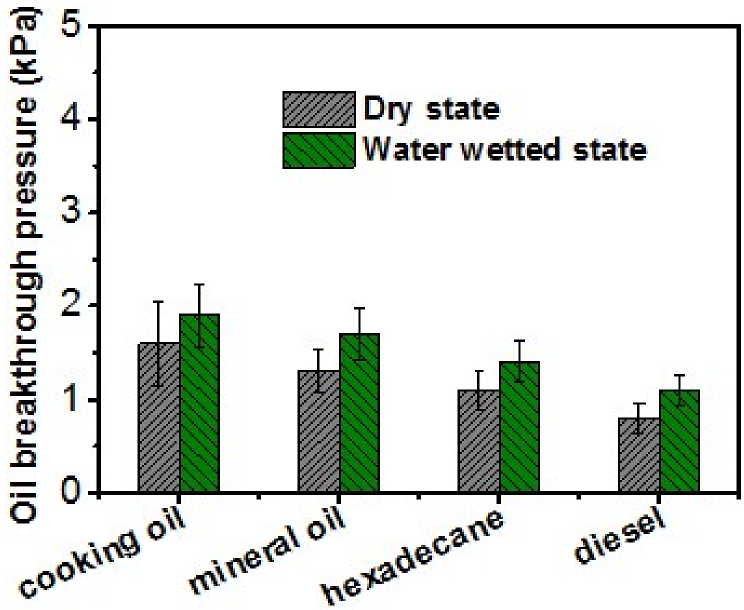

Fig. S14 Oil breakthrough pressures of uncoated membranes in dry and water wetted conditions.

In dry state, the membrane is oleophilic, with the breakthrough pressure ($P_{oil}$) of 1.6 kPa, 1.3 kPa, 1.1 kPa, and 0.8 kPa for cooking oil, mineral oil, hexadecane, and diesel, respectively. For the water wetted membrane, it corresponding $P_{oil,}$ was 1.9 kPa, 1.7 kPa, 1.4 kPa, and 1.1 kPa.

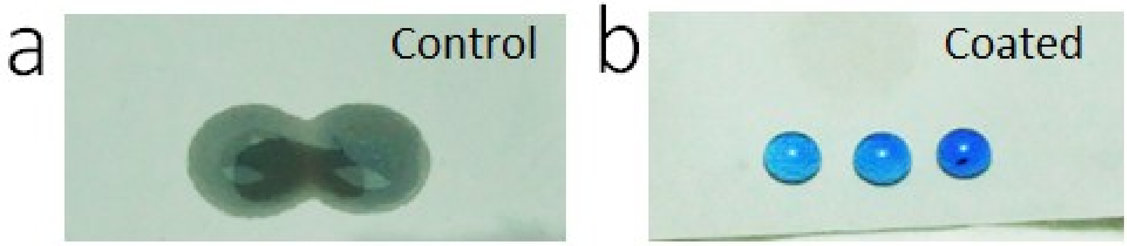


Fig. S15 Dropping PAO-4 (15 μL each droplet) on the a) control membrane, and b) coated membranes.

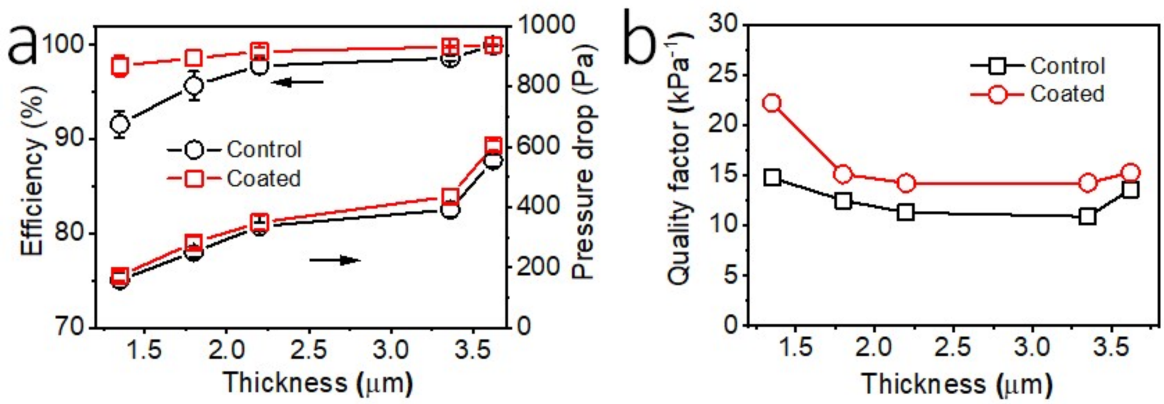


Fig. S16 The effect of the SHI-SOP membrane thickness on (control) a) oil aerosol filtration performance (efficiency and pressure drop) under flow rate of 10 m/s, b) quality factor at 10 cm/s flow rate.

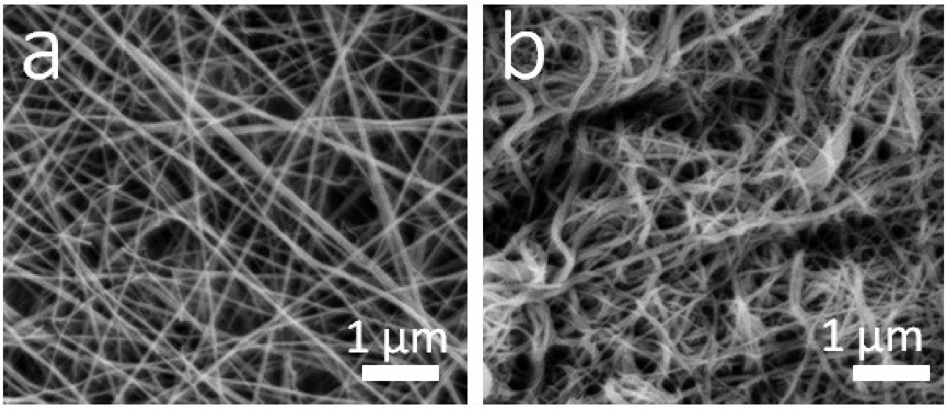

Fig. S17 SEM images of the nylon-6 nanofiber membrane: a) control sample with average pore size of 1.12 µm, b) after isopropanol treatment, the pore size down to around 0.82 µm.

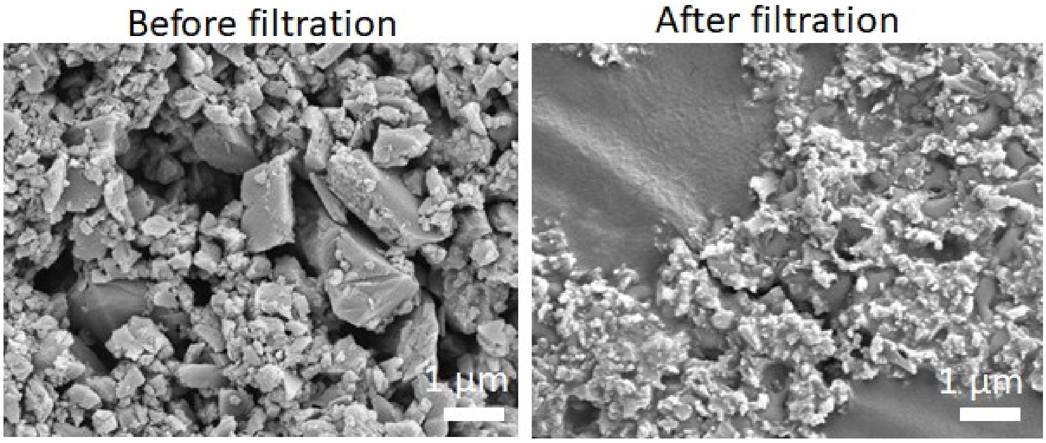


Fig. S18 SEM images of the $CaCO_3$ particles before and after the filtration.

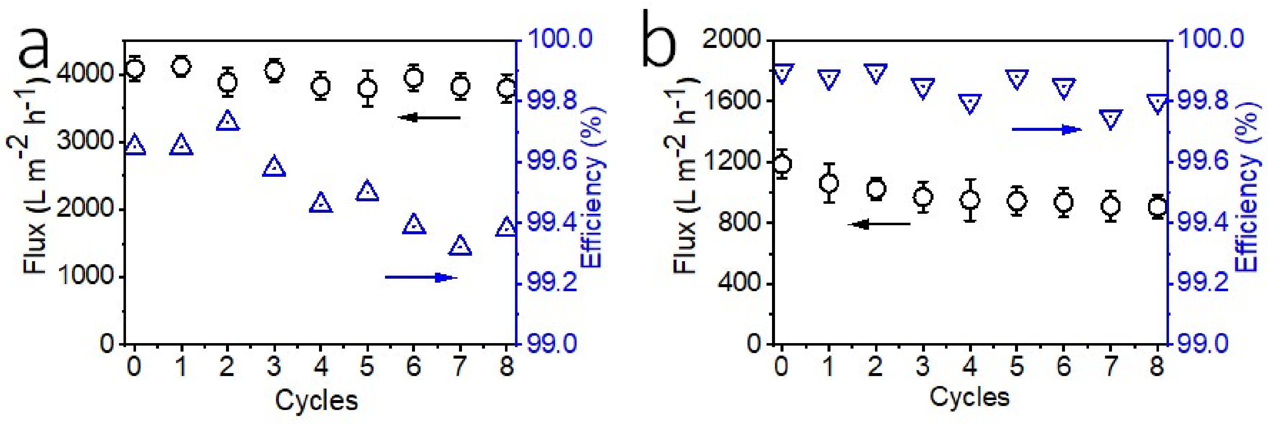


Fig. S19 Change of permeation fluxes with separation cycles (diesel based emulsions) for separation of a) SF and b) SS emulsions using the SHI-SOP membrane (the thickness 1.8 μm). In each cycle, 10 mL emulsion was used, and the membrane after separation was washed with water and dried in air.

The reusability of the membrane for emulsion separation was evaluated, using cooking oil emulsion as a model. The fibrous membrane can be used for multiple cycles. After 8 cycles of separation and washing, the membrane showed almost very small decay in separation performance for both SF and SS emulsions.

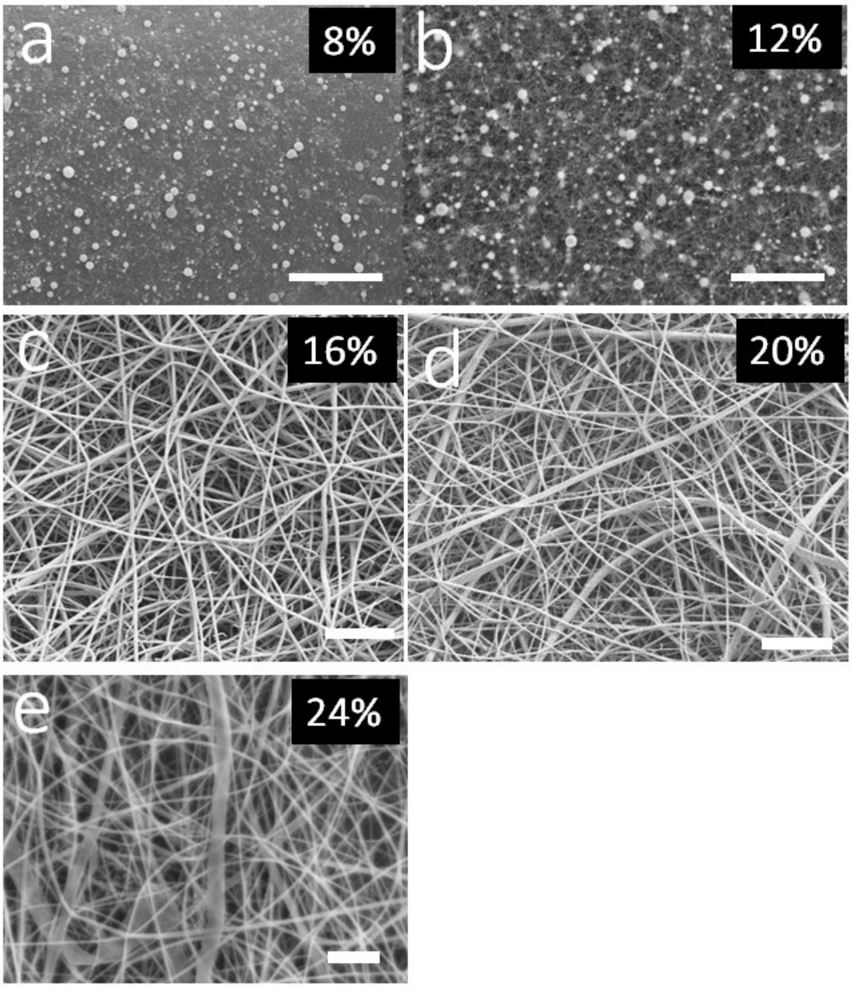


Fig. S20 SEM images of the Nylon6 nanofiber membranes derived from Nylon6 solution with different concentration: a) 8 wt%, b) 12 wt%, c) 16 wt%, d) 20 wt%, and 24% (scale bar=1μm).

Nylon-6 solutions with nylon-6 concentrations of 8, 12, 16, 20, and 24 wt% were used for electrospinning. Uniform nanofibers were prepared when the nylon-6 concentration was above 16 wt% (Fig. S2c). The nanofibers produced by 16 wt% nylon had an average diameter of 58±12 nm. They randomly deposited on the PET fabric to form a fibrous web. Higher Nylon-6 concentration resulted in increase of fiber diameter, to 85 nm for 24 wt% Nylon-6.

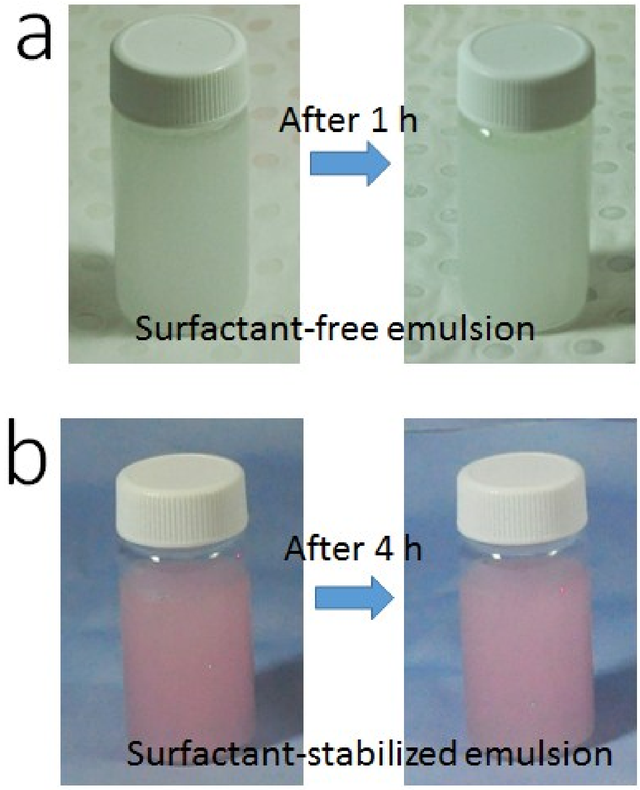


Fig. S21 Stabilities of the surfactant-free and surfactant-stabilized oil-in-water emulsions (from cooking oil).

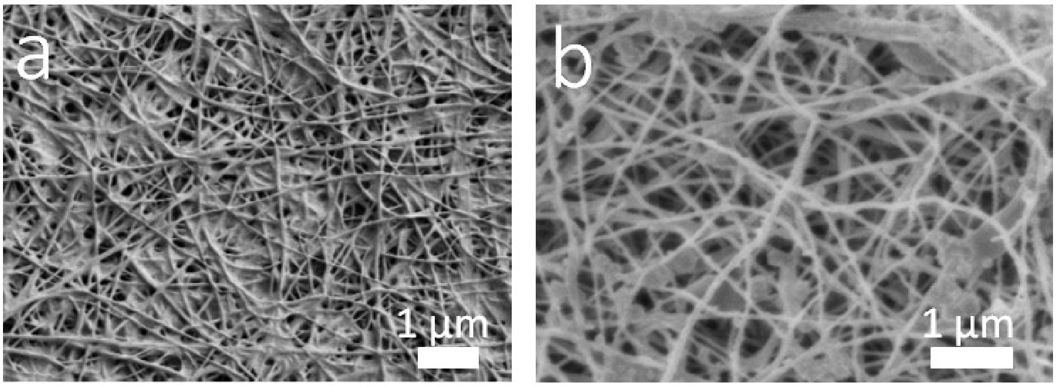


Fig. S22. SEM images of the nylon membrane after: a) diesel based SF oil-water emulsion separation, and b) aerosol NaCl separation.

Table S1. Wettability and filtration capability of filter materials

| Materials | Water wettability | Oil wettability | Underwater oil wettability | Oil/water emulsion separation | Solid/liquid separation | Oil/gas separation | Solid/gas separation |
|---|---|---|---|---|---|---|---|
| This work | Hydrophilic | Superoleophobic | Superoleophobic | High | High | High | High |
| Cellulose filter paper | Hydrophilic | Oleophilic | Oleophobic | × | Medium | Low | Low |
| PP nonwoven filter | Hydrophobic | Oleophilic | Oleophilic | × | Low | Low | Low |
| PET filter | Hydrophobic | Oleophilic | Oleophilic | × | Low | Low | Low |
| PVDF nanofiber web | Hydrophobic | Oleophilic | Oleophilic | Medium | × | Medium | Medium |
| Glass fiber filter | Hydrophilic | Oleophilic | Oleophobic | × | Medium | Medium | High |
| PTFE membrane | Hydrophobic | Oleophilic | Oleophilic | Medium | × | High | High |
| PAN membrane | Hydrophilic | Oleophilic | Oleophobic | Low | Medium | Medium | Medium-High |
| PVC membrane | Hydrophobic | Oleophilic | Oleophilic | Low | × | Medium | Medium |
| PES membrane | Hydrophobic | Oleophilic | Oleophilic | Low | × | Medium | Medium |
| PSF membrane | Hydrophobic | Oleophilic | Oleophilic | Low | × | Medium | Medium |
| PS membrane | Hydrophobic | Oleophilic | Oleophilic | Low | × | Medium | Medium |
| Ceramic membrane | Hydrophilic | Oleophilic | Oleophobic | Low | Medium-High | Medium | Medium-High |

Table S2. Summary of the oil properties

| Oils | Viscosity (mPa.s) | Density (mNm$^{-1}$) | Surface tension (mNm$^{-1}$) |
|---|---|---|---|
| Cooking oil | 43.7 | 0.96 | 32.0 |
| Mineral oil | 20 | 0.85 | 30.8 |
| Diesel | 3.5 | 0.92 | 28.4 |
| Hexadecane | 3.3 | 0.77 | 27.5 |

Table S3. Summary of the reported oil-in-water emulsion separation membranes

| Membrane types (surface wettability) | Oil-in-water emulsions | Permeation flux ($L/m^2.h$) | Feed pressure aid | Separation efficiency (%) | Ref |
|---|---|---|---|---|---|
| PVA nanocomposite layer/PVA nanofibrous layer/nonwoven support layer | Surfactant Stabilized (SS) | 330 | 68.9 kPa | Not provided | [1] |
| PVA hydrogel coating/PVA nanofiber nanocomposite ultrafiltration (UF) membrane | SS | <300 | 68.9 kPa | 99.5 | [2] |
| PVA hydrogel coating/PVA nanofiber/PET nonwoven substrate UF membrane | SS | <200 | 206.7 kPa | Not provided | [3] |
| Ceramic microfiltration (MF) membrane | Surfactant Free (SF) | <300 | 100-200 kPa | 90-99 | [4] |
| Polysulfone/bentonite nanoparticles composite MF membrane | SF | <300 | 300 kPa | ~95 | [5] |
| PVA/PAN composite nanofiber membrane | SS | ≤ 2100 | 300 kPa | 99.5 | [6] |
| Carbon nanotube/$TiO_2$ Ultrathin network films | SS | 14880 for diesel; 10320 for cooking oil | 100 kPa | 99.99 | [7] |
| Superamphiphilic PVDF membrane | SS | 9860 for cooking oil | 90 kPa | 99.96 | [8] |
| Superhydrophilic underwater superoleophobic silica nanofiber membrane | SS | 2237 for petroleum ether | Under gravity (1kPa) | — | [9] |
| Superhydrophilic underwater superoleophobic PAA-g-PVDF membrane | SS<br><br>SS | 2320 for hexadecane<br><br>570 for hexadecane | 10 kPa<br><br>Gravity (1kPa) | 99.99 | [10] |
| Superhydrophilic underwater superoleophobic Single-walled carbon nanotube based membrane | SS | 35890 for Chloroform | 100 kPa | 99.99 | [11] |
| Superhydrophobic and superoleophobic PVDF membrane | SF<br><br>SS | Up to 3415<br><br>700-1000 | Under gravity (1kPa) | >99.9 | [12] |
| Superhydrophilic underwater | SF | 2585 for hexadecane, 2371 | | >99.9 | [13] |

| | | | | | |
|---|---|---|---|---|---|
| superoleophobic PAN nanofibrous membrane | SS | for diesel;<br><br>1046 for hexadecane, 1100 for diesel; | Under gravity (1kPa) | | |
| Hydrolyzed PAN/GO composite nanofibrous membrane | SF | Up to 3500 | Under gravity (1kPa) | 99 | [14] |
| Superhydrophilic underwater superoleophobic PAN nanofibrous composite membrane | SF<br><br>SS | 2877 for cooking oil, 1984 for diesel;<br><br>410 cooking oil, 312 diesel; | under gravity (1kPa) | 99.93 | [15] |
| Our membrane: amphibious SHI-SOP with ultrathin nanofibrous composite structure | SF<br><br>SS | 4082 for diesel, 3182 for cooking oil<br><br>1183 for diesel, 847 for cooking oil | Under gravity (1kPa) | 99.65<br><br>99.9 | This work |

Table S4. Summary of the reported oil mist aerosol filtration membranes

| Membrane type | Thickness (μm) | Oil droplet size (nm) | Air flow rate | Filtration efficiency (%) | Pressure drop (kPa) | Quality factor ($kPa^{-1}$) | Ref |
|---|---|---|---|---|---|---|---|
| Stainless Steel 316 | 9000 | 850 ±17 | 55 $Lmin^{-1}$ | >90 | 1.36 | Not provided | [16] |
| Polypropylene +B-glass fibers | 14000 | 200-300 | 0.6 m/s | 93.16 | 5.32 | 0.76 | [17] |
| Polyester | 6240 | 40-295 | 1 m/s | 75-95 | 0.6 | Not provided | [18] |
| Glass + polypropylene | 14000 | 200-300 | 0.6 m/s | 93.38 | 4.68 | 0.77 | [19] |
| Glass fiber + polyamide nanofiber | Not provided | 210 | 188 $Lmin^{-1}$ | 98.9 | 13 | 0.38 | [20] |
| Bioactive nonwoven + Polypropylene | 1660 | 600 | 30 $Lmin^{-1}$ | 97.7 | Not provided | Not provided | [21] |
| Stainless steel filter | 10000 | 400 | 0.1 m/s | 87 | 0.131 | 15.54 | [22] |
| Glass fiber filter | 2240 | 10-800 | 127.2 $Lmin^{-1}$ | 99.96 | 9.94 | 0.78 | [23] |
| B-glass fibers + Teflon | 14000 | 10-800 | 0.6 m/s | 99.75 | 3.53 | 1.60 | [24] |
| Glass fiber | 5000 | 640 | 0.7 m/s | 99.99 | 8.5 | Not provided | [25] |
| Fibrous filter | 680 | < 1000 | 0.21 m/s | 58 | 2.4 | Not provided | [26] |
| Fibrous filter | Not provided | <500 | 0.1 m/s | 90 | 26.9 | Not provided | [27] |
| Fibrous filter + mesh | 3000 | < 1000 | 10.7 $Lmin^{-1}$ | 99.5 | 6 | Not provided | [28] |
| FS-60 coated nylon nanofiber membrane work | 1.1~3.75 | ~330 | 0.1m/s | Up to 99.98% | < 0.6 | >20 | This work |

References


[S 1] X. Wang, X. Chen, K. Yoon, D. Fang, B. S. Hsiao, B. Chu, *Environmental Science & Technology* **2005**, 39, 7684.

[S 2] X. Wang, D. Fang, K. Yoon, B. S. Hsiao, B. Chu, *Journal of Membrane Science* **2006**, 278, 261.

[S 3] Z. Tang, J. Wei, L. Yung, B. Ji, H. Ma, C. Qiu, K. Yoon, F. Wan, D. Fang, B. S. Hsiao, B. Chu, *Journal of Membrane Science* **2009**, 328, 1.

[S 4] S. Emani, R. Uppaluri, M. K. Purkait, *Ceramics International* **2014**, 40, 1155.

[S 5] S. Kumar, C. Guria, A. Mandal, *Separation and Purification Technology* **2015**, 150, 145.

[S 6] X. Wang, K. Zhang, Y. Yang, L. Wang, Z. Zhou, M. Zhu, B. S. Hsiao, B. Chu, *Journal of Membrane Science* **2010**, 356, 110.

[S 7] S. J. Gao, Z. Shi, W. B. Zhang, F. Zhang, J. Jin, *ACS Nano* **2014**, 8, 6344.

[S 8] T. Mimi, X. Lixin, L. Fu, J. Lei, *Advanced Materials* **2014**, 26, 2943.

[S 9] S. Yang, Y. Si, Q. Fu, F. Hong, J. Yu, S. S. Al-Deyab, M. El-Newehy, B. Ding, *Nanoscale* **2014**, 6, 12445.

[S 10] W. Zhang, Y. Zhu, X. Liu, D. Wang, J. Li, L. Jiang, J. Jin, *Angewandte Chemie International Edition* **2014**, 53, 856.

[S 11] L. Hu, S. Gao, X. Ding, D. Wang, J. Jiang, J. Jin, L. Jiang, *ACS Nano* **2015**, 9, 4835.

[S 12] Z. Wenbin, S. Zhun, Z. Feng, L. Xia, J. Jian, J. Lei, *Advanced Materials* **2013**, 25, 2071.

[S 13] J. Ge, J. Zhang, F. Wang, Z. Li, J. Yu, B. Ding, *Journal of Materials Chemistry A* **2017**, 5, 497.

[S 14] J. Zhang, X. Pan, Q. Xue, D. He, L. Zhu, Q. Guo, *Journal of Membrane Science* **2017**, 532, 38.

[S 15] G. Jianlong, Z. Dingding, J. Qing, Y. Jianyong, D. Bin, *Advanced Functional Materials* **2018**, 28, 1705051.

[S 16] A. Bredin, B. J. Mullins, *Separation and Purification Technology* **2012**, 90, 53.

[S 17] S. U. Patel, P. S. Kulkarni, S. U. Patel, G. G. Chase, *Drying Technol.* **2013**, 31, 185.

[S 18] T. Jankowski, *Fib. Text. East. Euro* **2009**, 17, 87.

[S 19] S. U. Patel, G. G. Chase, *Separation and Purification Technology* **2010**, 75, 392.

[S 20] M. G. Hajra, K. Mehta, G. G. Chase, *Sep. Purif. Technol.* **2003**, 30, 79.

[S 21] K. Majchrzycka, B. Gutarowska, A. Brochocka, B. Brycki, *International Journal of Occupational Safety and Ergonomics* **2012**, 18, 375.

[S 22] G. M. Manzo, Y. Wu, G. G. Chase, A. Goux, *Sep. Purif. Technol.* **2016**, 162, 14.

[S 23] X. Wei, F. Chen, H. Wang, H. Zhou, Z. Ji, T. Lin, *Journal of Materials Chemistry A* **2018**, 6, 871.

[S 24] S. U. Patel, P. S. Kulkarni, S. U. Patel, G. G. Chase, *Separation and Purification Technology* **2012**, 87, 54.

[S 25] H. E. Kolb, J. Meyer, G. Kasper, *Chem. Eng. Sci.* **2017**, 166, 107.

[S 26] A. Charvet, Y. Gonthier, A. Bernis, E. Gonze, *Chem. Eng. Res. Des.* **2008**, 86, 569.

[S 27] S. Fotovati, H. Vahedi Tafreshi, B. Pourdeyhimi, *Chemical Engineering Science* **2010**, 65, 5285.

[S 28] B. J. Mullins, R. Mead-Hunter, R. N. Pitta, G. Kasper, W. Heikamp, *AIChE Journal* **2014**, 60, 2976.